AIAA JOURNAL
Vol. 45, No. 8, August 2007

Dual Location Separation Control on a Semispan Wing

David Greenblatt*
Berlin University of Technology, 10623 Berlin, Germany

DOI: 10.2514/1.27757

Separation is controlled on a semispan wing via nominally two-dimensional zero mass-flux perturbations that are introduced at 1) the leading edge, 2) the shoulder of deflected flaps (20–40 deg deflection), and 3) both locations simultaneously. Leading-edge perturbations mimic the effect of a leading-edge device and flap-shoulder perturbations simulate additional flap deflection while simultaneously reducing drag. When perturbations are introduced simultaneously, at reduced frequencies of O(1) at poststall angles of attack, their combined effect on the wing's lift exceeds each individual contribution. When the physical frequencies are the same, lift is strongly dependent on the difference in phase between the two perturbations and an optimum is reached when the suction portion of flap-shoulder control coincides with the minimum shear layer proximity to the flap surface. At the optimum phase difference, increases in lift are observed over the entire semispan, resulting in an overall increase in the wing maximum lift coefficient between 0.24 and 0.44 depending on the flap deflection configuration and angle. Flap-shoulder control effectiveness does not diminish at the extremities of the finite inboard flap; neither inboard in the vicinity of the junction vortex, nor outboard in the vicinity of the flap-edge vortex. With a large flap deflection across the entire span, flap-shoulder control perturbations produce a powerful tip vortex that may be exploited for lift enhancement on low aspect ratio wings. The sensitivity to perturbation phase difference, however, diminished significantly toward the wing tip.

Nomenclature

C_D	=	wing form-drag coefficient
C_d	=	sectional form-drag coefficient
C_L	=	wing lift coefficient
C_l	=	sectional lift coefficient
C_M	=	wing moment coefficient
C_m	=	sectional moment coefficient
C_p	=	time-mean pressure coefficient
C_μ	=	slot momentum coefficient, $h/c(U_j/U_\infty)^2$
c	=	wing chord length
F^+	=	reduced excitation frequency, fX/U_∞
f	=	separation control excitation frequency
h	=	slot width
L_f	=	flap length, from slot to trailing edge
q	=	freestream dynamic pressure
Re	=	Reynolds number based on chord length
s	=	wing semispan length, $b/2$
U, V, W	=	mean velocities in directions x, y, z
U_j	=	peak jet slot blowing velocity
U_∞	=	freestream velocity
X	=	distance from perturbation to wing trailing edge
x, y, z	=	coordinates measured from model leading edge and root (left-hand system)
α	=	angle of attack
α_s	=	static stall angle
δ_f	=	flap deflection angle
ξ, ζ	=	local flap coordinate system
Ω_y	=	spanwise vorticity
$\langle\,\rangle$	=	phase-averaged quantity

Subscripts

i	=	inboard
fs	=	flap shoulder
le	=	leading edge
o	=	outboard
t	=	tip
te	=	trailing edge

Presented as Paper 5085 at the 23rd AIAA Applied Aerodynamics Conference, Westin Harbour Castle, Toronto, Ontario, Canada, 6–9 June 2005; received 11 September 2006; revision received 7 February 2007; accepted for publication 9 February 2007.

*Senior Research Scientist, Institute of Fluid Dynamics and Engineering Acoustics, Berlin University of Technology, 8 Mueller Breslau Street, 10623 Berlin, Germany. Senior Member AIAA.

I. Introduction

ALTHOUGH periodic excitation has long been recognized as an effective means for delaying separation (see review in [1]), it was only relatively recently demonstrated at flight Reynolds numbers [2] and in full-scale flight tests [3]. Perturbations can take the form of zero or nonzero net mass-flux oscillatory blowing, surface-mounted actuators, or a combination of the two. One of the major objectives of active separation control research is to provide a viable simplified alternative to present-day high-lift systems. The basic idea is to replace complex high-lift system components, totally or partially, with simple flaps and leading-edge droop, and then control separation by means of autonomous actuators [1].

A central challenge is the optimization of control to yield the maximum beneficial results with the lowest associated cost. One approach to the problem is to introduce perturbations at multiple locations or at multiple frequencies and then optimize the control. It has been noted previously [4,5] that the growth of a mixing layer can be profoundly affected by simultaneous excitation at two frequencies, namely the fundamental excitation frequency f and the subharmonic frequency $f_s = 1/2f$, by varying their relative amplitudes. Also, mean flow distortion can be attained by introducing two spinning waves into an axisymmetric jet, where the distortion is altered by varying the phase difference [6]. It was recently shown [7] that pulse modulated perturbations from two neighboring slots on an airfoil can interact favorably to increase lift. In addition, perturbations from remote slots, namely a leading-edge slat and a flap, were more beneficial than their individual contributions. The effect of phasing the perturbations from remote slots was not reported.

Another challenge to simplified high-lift is the effect of geometric or flow three-dimensionality. Very little is known of the efficacy of control near flap edges, wing tips, or wing–body junctions. The bulk of experimental data is for two-dimensional geometries, although the effect of infinite sweep has been studied [8] and control has also been demonstrated on delta wings [9]. The flow near flap edges, unlike wing tips, is often separated and strong three-dimensionality is present in the form of flap-edge vortices [10]. The flap-edge three-dimensionality may enhance control to some degree because the flap-edge vortex aids in the transfer of high-momentum fluid to the upper surface from below the wing. Control is then the result of a combination of spanwise vortices produced by excitation of the free shear layer superimposed approximately orthogonally on the flap-edge vortex [11]. In contrast, inboard control terminates at the junction between the tunnel wall (or body), where a horseshoe vortex is formed [12]. Consequently, no fluid can be drawn from the lower part of the wing and control effectiveness may decrease as the separation control perturbations become less two-dimensional when they interact with the junction vortex.

This paper reports on a pilot wind-tunnel investigation that was intended as a precursor to more detailed studies on simplified high-lift systems. Three aspects of separation control were studied. The first aspect considered the efficacy of separation control on a finite flap geometrically bounded inboard by a wing/tunnel-wall junction and outboard by the flap edge. The second aspect involved the effect of excitation at two remote locations (namely at the leading edge and the shoulder of a deflected flap) and at both locations simultaneously. A main objective of this aspect was an attempt at aerodynamic load optimization resulting from the phase difference between the perturbations introduced at the two locations. Finally, a "simplified high-lift" configuration was studied, involving a large flap deflection along the entire span with separation control introduced at both the leading edge and flap shoulder.

II. Rationale for Dual Location Perturbations

The basis for this approach is the observation that perturbations introduced at or near a separation point amplify and roll up into discrete spanwise vortices. This is illustrated, for example, by the stereoscopic particle image velocimetry (PIV) flowfield measurements in a separated flow controlled by two-dimensional perturbations [13]. It is observed that forcing accelerates and regulates the generation of large coherent structures, particularly when the mean flow is unstable, thereby transferring high-momentum fluid across the mixing layer, toward the surface.

With increasing frequency, the rolled-up vortices amplify over a shorter distance from the slot and thus the perturbations dissipate closer upstream, resulting in diminished separation control effectiveness. When the frequency is reduced, the rolled-up vortices amplify over a longer distance and, ultimately, if the amplification rate is too low, control effectiveness diminishes. As a consequence of these conflicting mechanisms, the optimum reduced frequencies for separation control fall within the approximate range of $0.3 \leq F^+ \equiv fX/U_\infty \leq 3$, providing a minimum perturbation amplitude is exceeded, typically $C_\mu \geq 0.1\%$.

The rationale behind the present approach is explained with reference to Figs. 1 and 2. The figures show schematics of an airfoil at

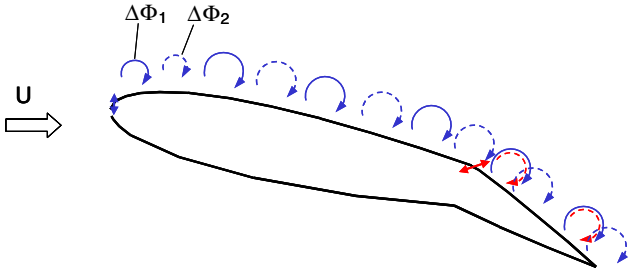

Fig. 1 Conceptual model of spanwise rolled-up vortices generated via forcing at the leading edge and flap shoulder.

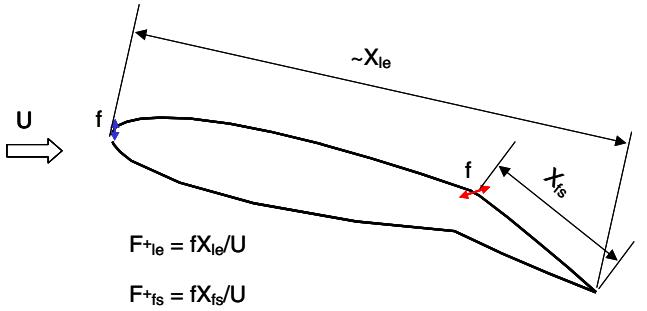

Fig. 2 Definitions of length scales traditionally used for separation control.

a positive angle of attack with a deflected flap, where perturbations are introduced from the leading edge and flap shoulder simultaneously. If the vortices generated by perturbations from the leading edge and flap shoulder do not interact, and the flow is attached upstream of the flap, then the net effect of each can be considered independently. Consider, however, the conceptual model of spanwise rolled-up vortices as they are generated and advected over the airfoil surface. If we assume that the velocity perturbation at the leading edge is represented by

$$u_{j,\mathrm{le}} = U_{j,\mathrm{le}} \sin(\omega_{\mathrm{le}} t - \phi_{\mathrm{le}}) \tag{1}$$

and that at the flap shoulder is represented by

$$u_{j,\mathrm{fs}} = U_{j,\mathrm{fs}} \sin(\omega_{\mathrm{fs}} t - \phi_{\mathrm{fs}}) \tag{2}$$

then we can define a phase difference between the two as $\Delta\phi = \phi_{\mathrm{fs}} - \phi_{\mathrm{le}}$. For simplicity, we further assume that $f_{\mathrm{fs}} = f_{\mathrm{le}} = f$, where $\omega = 2\pi f$. Given constant $U_{j,\mathrm{le}}$, $U_{j,\mathrm{fs}}$, and f, Fig. 1 illustrates two scenarios for simultaneous forcing from the two locations at distinct phase differences, namely $\Delta\phi_1$ and $\Delta\phi_2$. The figure illustrates that changing the relative phase of the perturbations can result in substantially different interaction of the vortices over the airfoil flap. For this conceptual model to be applicable, three physical requirements should be met. First, the vortices that result from the leading-edge perturbations should maintain a substantially two-dimensional nature up to the flap shoulder. Second, the reduced frequencies based on the leading-edge ($F^+_{\mathrm{le}} \equiv fX_{\mathrm{le}}/U_\infty$) and flap-shoulder ($F^+_{\mathrm{fs}} = fX_{\mathrm{fs}}/U_\infty$) length scales should be in the appropriate range for effective separation control. Third, the vortices arising from leading-edge forcing should not dissipate to a state in which they are too weak to have a meaningful interaction with the flap-shoulder generated vortices. Finally, it can be appreciated from Fig. 2 that because, in general, $X_{\mathrm{le}} \neq X_{\mathrm{fs}}$, then $F^+_{\mathrm{le}} \neq F^+_{\mathrm{fs}}$.

III. Experimental Setup

Experiments were performed on a rectangular planform semispan NACA 0015 portside wing of aspect ratio AR = 4 (semispan $s = 609.6$ mm, chord $c = 304.8$ mm) cantilever-mounted in the NASA Langley Research Center (LaRC) Basic Aerodynamics Research Tunnel. The wing has a main element and three identical simple flaps of span $s_f = 1/3s$ hinged at $0.7c$. Two configurations were considered in this study: two inboard flaps ($2/3s$) deflected to 20 deg (see photograph in Fig. 3a), and all flaps deflected to 20 and 40 deg. The wing is equipped with two independently operated forcing slots, namely a leading-edge slot (Fig. 3b) and a flap-shoulder slot (Fig. 3a). Forcing was supplied to fore and aft interior plenums, respectively, via externally mounted, voice-coil based actuators (see Fig. 4).

The model is further equipped with 165 static pressure ports arranged in a perpendicular spanwise and chordwise grid, where surface pressures were integrated to estimate aerodynamic loads. The spanwise ports are located at the chordwise locations $x/c = 0.005$, 0.3, 0.77, and 1, and are grouped more closely near the tip. The chordwise ports are located at spanwise locations $y/s = 0.167$, 0.5, 0.833, and 0.99, and are grouped more closely near the leading edge.

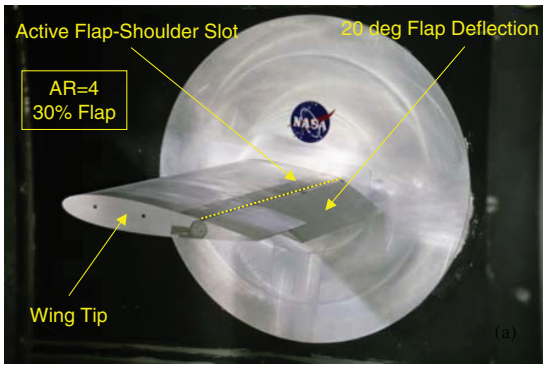

a)

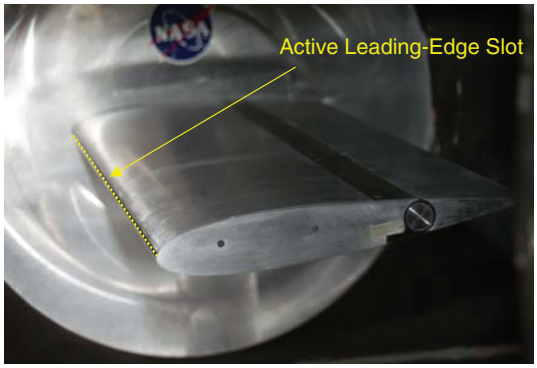

b)

Fig. 3 Two views of NACA 0015 semispan model installed in the basic aerodynamics research tunnel.

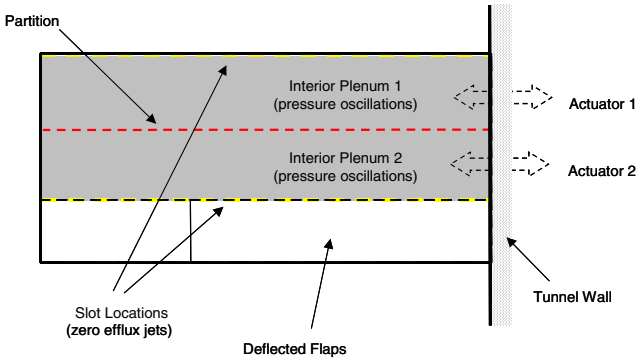

Fig. 4 Semispan model cutaway plan view.

Ports are also located close to the flap edges. The model is also equipped with unsteady pressure transducers; nine are mounted on the wing upper surface and three are mounted within the wing plenums. Wing static pressures were measured using a high-speed pressure scanner and unsteady pressures were measured by means of piezoresistive unsteady pressure transducers. The main source of error in the pressure measurements was due to precision, with $\Delta C_p \leq \pm 0.02$, based on 95% confidence intervals. Peak slot velocities were calibrated using a hot wire anemometer and maximum uncertainties were estimated at $\Delta C_\mu / C_\mu \leq 20\%$.

Two-dimensional PIV was employed to measure the flowfield above the flap in the (x, z) plane corresponding to the model center span ($y/s = 0.5$) for both baseline and controlled cases. The setup included an Nd:YAG double-pulsed 100 mJ laser and a 1024×1280 charged-coupled device (CCD) camera. Smoke particles (specific gravity 1.022) were generated by means of a standard smoke generator and the largest particles were on the order of 4–5 μm as measured by a commercial aerodynamic particle sizer. Data processing was performed using 28×28 pixel interrogation areas corresponding to 1×1 mm with a 50% overlap. For the control cases, data were acquired and averaged at 10 phases of the control cycle. The time delay between image pairs was set to allow a maximum particle displacement of one-third of the interrogation area (typically 9 pixels) and 400 image pairs were acquired at each phase. Resolution and precision errors (based on 95% confidence intervals) were estimated as 1.3 and 1%, respectively, for U/U_∞ and V/U_∞.

IV. Discussion of Results

A. Leading-Edge Control

On determining that the wing stalls inboard at $\alpha \approx 13$ deg (shown later), the wing was set at poststall angle ($\alpha = 16$ deg) and the effect of forcing at various frequencies and amplitudes was considered. The results of C_l at $y/s = 0.167$ are shown in Fig. 5, as a function of $F_{le}^+ = fX_{le}/U_\infty$, for three values of C_μ. All C_l data are obtained by integrating the surface pressures at $y/s = 0.167$. The general trends are similar to those observed on the Tel-Aviv University (TAU) NACA 0015 airfoil, also shown in the figure [1], with optimum conditions approximately at $0.5 < F_{le}^+ < 2$. Increasing C_μ results in a larger effective F_{le}^+ range, which is also consistent with airfoil data [1]. However, in both the TAU airfoil data and NASA Langley Research Center wing data, lift did not increase proportionately with C_μ (not shown). These nonlinearities were attributed to the combination of transitional flow at the leading edge and the high degree of surface curvature just downstream of the slot. It should further be appreciated that when flow is attached to the main element by leading-edge forcing, it separates at the flap shoulder. Consequently, it may be more appropriate to use the length scale $X_{le} - X_{fs}$ instead of X_{le} in the F_{le}^+ definition, resulting in a shift to the left of the NASA Langley Research Center data in Fig. 5 and better agreement between the two data sets.

To apply control at both the leading edge and the flap shoulder simultaneously, we need to recognize that $F_{fs}^+ = fX_{fs}/U_\infty = f(0.3X_{le})/U_\infty$ and consequently $F_{fs}^+ = 0.3F_{le}^+$. Thus, an effective F_{le}^+ will not necessarily result in an effective F_{fs}^+, and this is illustrated by the corresponding F_{fs}^+ abscissa in Fig. 5. The increased effective F_{le}^+ range at $C_\mu = 0.3\%$ provides an opportunity to obtain reduced frequencies that are effective for forcing from both locations, namely $1.0 \leq F_{le}^+ \leq 2.5$ and $0.3 \leq F_{fs}^+ \leq 0.75$, corresponding to the same physical frequency in the range of $80 \leq f \leq 200$ Hz. It is known, however, that as F_{le}^+ increases, we can expect the rolled-up vortices to amplify over a shorter distance from the slot and thus the perturbations will dissipate closer upstream as compared with those generated at lower F_{le}^+. Because the leading-edge vortices decay more readily at higher frequencies, they may decay below the threshold required for a meaningful interaction with the flap vortices.

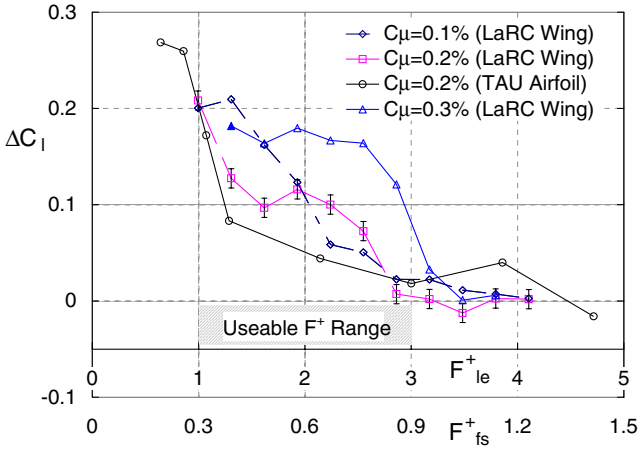

Fig. 5 Inboard poststall lift coefficient data with leading-edge control (inboard flaps deflected 20 deg); LaRC $Re = 500,000$, TAU airfoil $Re = 200,000$.

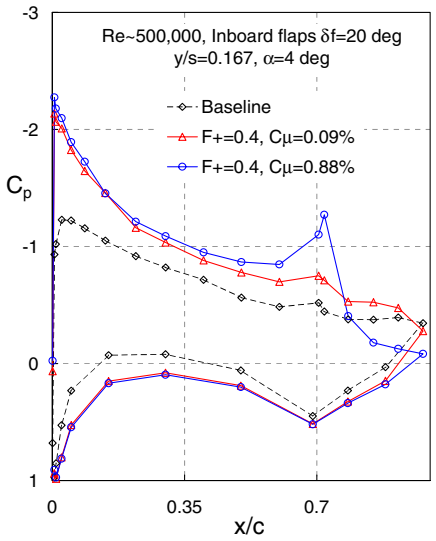

Fig. 6 Inboard pressure coefficient distribution for flap-shoulder control ($F^+_{fs} = 0.4, f = 105$ Hz corresponding to $F^+_{le} = 1.3$).

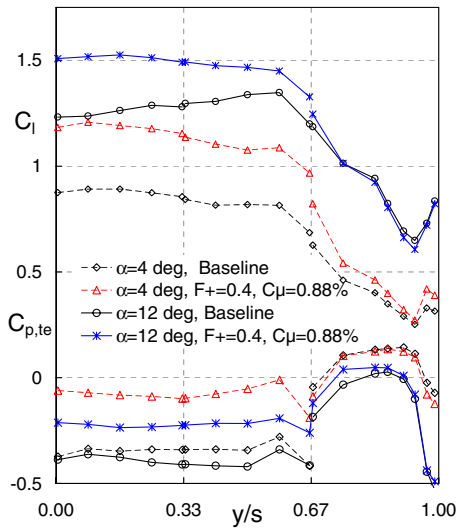

Fig. 7 Span-loading and trailing-edge pressure coefficients for flap-shoulder control at two angles of attack ($Re = 500,000$).

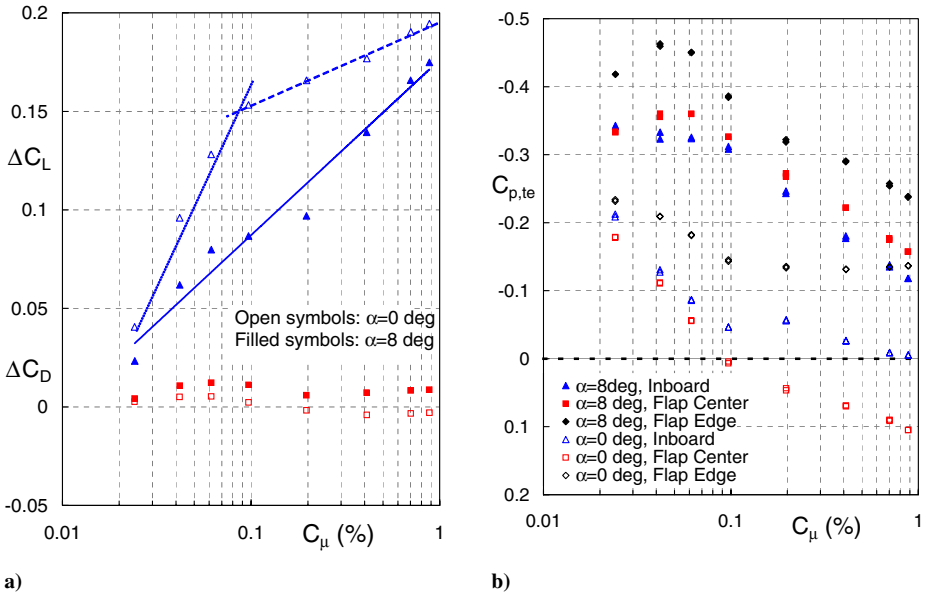

a) b)

Fig. 8 Changes to aerodynamic coefficients and representative trailing-edge pressures for a) lift and form drag coefficients, and b) "control effectiveness" as a function of flap-shoulder control momentum coefficient ($Re = 500,000$).

B. Flap-Shoulder Control

Based on the preceding observations, data with flap-shoulder control were acquired for the range of reduced frequencies $0.3 \leq F^+_{fs} \leq 0.75$; a typical example ($F^+_{fs} = 0.4$) is shown in Figs. 6–9. Inboard ($y/s = 0.167$), separation control behaves similarly to that on an airfoil (Fig. 6) [1], where control manifests as an increase in circulation on the inboard portion of the wing. An order of magnitude increase in C_μ results in enhanced separation control on the flap, but a small increase in circulation (or lift). The effect of control on the finite flap is shown by the spanwise variation of C_l and $C_{p,te}$ at two angles of attack (Fig. 7). At relatively low angles of attack, the effect of control is approximately uniform across the flap span, as indicated by the changes to C_l and $C_{p,te}$. The relatively low trailing-edge pressures near the flap edge, with and without control, result from the flap-edge vortex. As the wing approaches α_s, stall commences inboard and, therefore, the effect of control on lift is larger in this region. For unsteady flows in general, and oscillatory separation control in particular, classical definitions of separation are not always appropriate for describing the observed effects. Control often produces flow states that are neither fully attached nor fully separated. In addition to the standard aerodynamic coefficients, we also consider the trailing-edge pressure coefficient to assess the "degree of flow separation" (relatively large negative $C_{p,te}$) and the effectiveness of separation control (flow is assumed to be attached when $C_{p,te} \geq 0$). Based on these considerations, we observe that at both $\alpha = 4$ and 12 deg the flow is not fully attached ($C_{p,te} < 0$), even at the highest control amplitude employed here (Figs. 6 and 7).

Wing aerodynamic coefficients and representative trailing-edge pressures are shown in Figs. 8a and 8b as a function of the control momentum coefficient; data as a function of α are shown in Figs. 9a and 9b (even angles are for α increasing and odd angles are for α decreasing). These data are broadly consistent with two-dimensional airfoil data: at $\alpha = 0$ deg, effective control over the flap requires a relatively small input ($C_\mu \sim 0.1\%$), whereas further increases in C_μ result in a lower dC_L/dC_μ (Figs. 8a and 8b); at larger angles of attack ($\alpha = 8$ deg), C_L increases gradually and approximately logarithmically with C_μ whereas C_D is not materially affected (Fig. 8a); relatively large perturbations ($C_\mu \sim 1\%$) are required to increase $C_{L,max}$ (Figs. 9a and 9b). Based on $C_{p,te}$ it was concluded that the flow is not fully attached at $\alpha > 2$ for the range of amplitudes considered

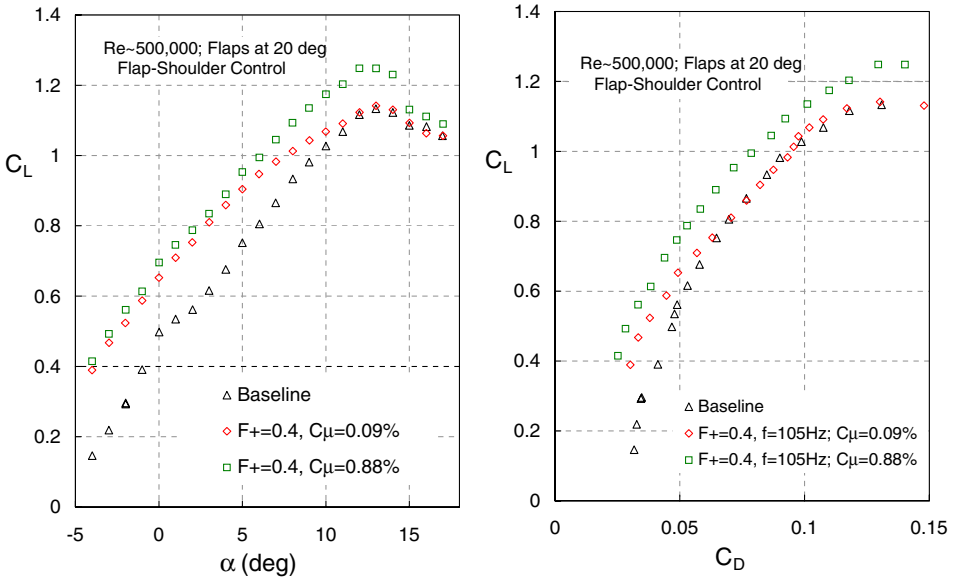

Fig. 9 Lift and form drag coefficients for flap-shoulder control.

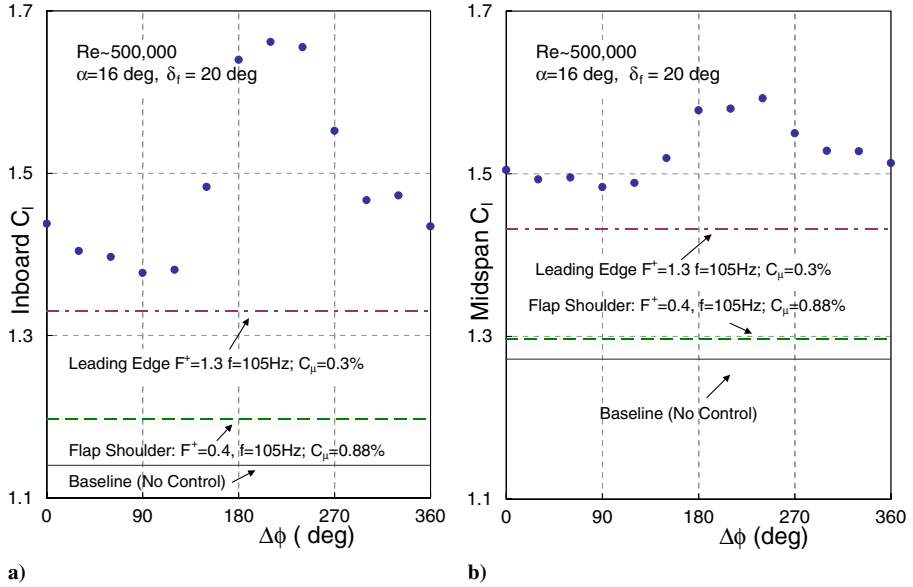

Fig. 10 Poststall lift coefficient data showing effect of phase when separation is controlled from two locations: a) inboard, and b) midspan.

here. Also note that at the flap edge $C_{p,\mathrm{te}} < 0$, irrespective of α or the control momentum, due to the existence of a flap-edge vortex. Note, however, that the existence of a vortex does not diminish the lift increment corresponding to the edge of the flap at $\alpha = 4$ deg(see Fig. 7). Also, the wing-junction vortex does not appear to significantly affect control effectiveness.

C. Combined Control

Figure 10a shows the two-dimensional lift coefficients $[C_l(y/s = 0.167)]$ for excitation from the slots individually as well as simultaneously at the same physical frequency ($f = 105$ Hz) at poststall conditions ($\alpha = \alpha_s + 3$ deg; $\alpha_s = 13$ deg). The solid horizontal line represents the baseline case, i.e., when no separation control is applied. The dashed and hatched lines represent the cases in which control is applied from the leading edge ($F^+_{\mathrm{le}} = 1.3$) and flap shoulder ($F^+_{\mathrm{fs}} = 0.4$), respectively. When perturbations are introduced simultaneously (data points), their combined effect on the sectional lift exceeds each individual contribution, i.e., the lift never falls below that generated by leading-edge control alone (here $\Delta\phi$ is based on the voltage drive signal). More important, the data show a marked sensitivity to phase difference, with minimum and maximum lift at approximately $60 < \Delta\phi < 120$ deg and $180 < \Delta\phi < 240$ deg, respectively. The lift disparity that results from the varying of phase difference alone is $\Delta C_l \approx 0.28$. A similar, but less pronounced, result can be seen at $y/s = 0.5$ in Fig. 10b.

Spanwise lift distributions are shown for the baseline case and combined control corresponding to the minimum and maximum lift enhancement (Fig. 11). The baseline data reflects inboard stall with decreased lift near the wing–tunnel-wall junction. Control at $\Delta\phi = 90$ deg increases lift approximately uniformly across the span. However, control at $\Delta\phi = 210$ deg brings about significant additional lift inboard, thereby restoring prestall-type lift distributions (cf. Fig. 7). Integration of the lift distributions, such as those shown in Fig. 11, allowed an assessment of the overall wing lift as a function of the phase difference (Fig. 12).

The inboard ($y/s = 0.167$) pressure distributions are shown in Fig. 13 for poststall baseline as well as the two phase differences

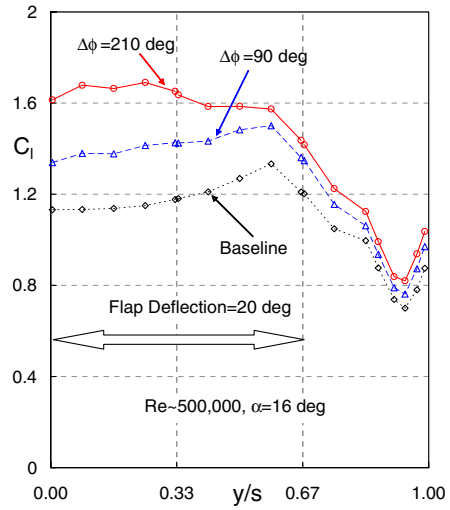

Fig. 11 Poststall wing span loading showing effect of phase difference when separation is controlled from two locations (control corresponds to Fig. 10).

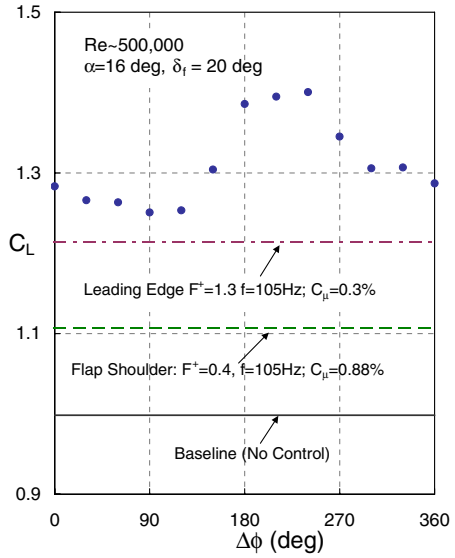

Fig. 12 Poststall total wing lift data showing effect of phase when separation is controlled from two locations.

$\Delta\phi = 90$ and $\Delta\phi = 210$ deg. Baseline data shows a typical stalled pressure distribution, with the separation location at $x/c \approx 0.25$. Control at $\Delta\phi = 90$ deg has an almost indiscernible effect on the flap C_p whereas that at $\Delta\phi = 210$ deg is clearly more noticeable, but still relatively small. The most significant effect is seen well upstream of the flap shoulder, e.g., leading edge $\Delta C_p \approx 0.1$, and this diminishes toward the flap shoulder. The relatively small changes to $C_{p,\text{te}}$ indicate that the flow is still far from being attached over the flap.

Phase-averaged, unsteady pressures in the fore and aft plenums (Figs. 14a and 14b) and unsteady surface pressures measured immediately downstream of the slots at $y/s = 0.167$ (Figs. 14c and 14d) are shown for leading edge, flap shoulder, and combined control. Combined control is shown for the phase differences corresponding to minimum and maximum lift enhancement. One effect of phase difference is clearly seen by comparing the leading-edge slot plenum unsteady pressures (Figs. 14a). For flap-shoulder control, the mean pressure is relatively high, consistent with the lower lift (e.g., Fig. 12) and shows no virtually no unsteady response, which is consistent with fully separated flow at the leading edge. For all other instances, the peak-to-peak amplitude is approximately the same because the input perturbation is the same, but the mean pressure associated with $\Delta\phi = 210$ deg is lower and this is again

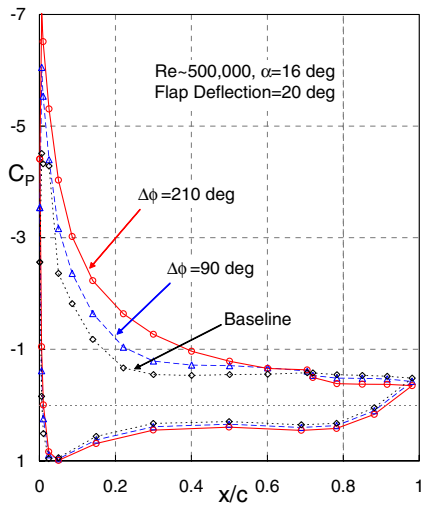

Fig. 13 Poststall inboard wing pressure distribution at $y/s = 0.167$ showing the effect of phase when separation is controlled from two locations.

consistent with higher lift (e.g., Fig. 12). This general description is also appropriate for the pressure measured just downstream of the leading-edge slot ($x/c = 0.005$, Fig. 14c), with one exception: the pressure oscillations are larger for $\Delta\phi = 210$ deg than for $\Delta\phi = 90$ deg. Similar observations were made at $x/c = 0.3$ (not shown). Control of separation is known to have a global effect on the mean pressure distribution as it affects the overall circulation [1]. The leading-edge pressure fluctuations (Fig. 14c) suggest that this global effect is not confined to the mean flow, but also manifests as an enhancement of the leading-edge perturbations. Hence, the ratio of unsteady pressure oscillation amplitude to time-mean pressure remains approximately constant.

Flap-shoulder plenum fluctuations show similar peak-to-peak fluctuations, with the exception of when no flap-shoulder control is applied and, hence, the plenum pressure responds only to the pressure fluctuations that result from leading-edge control (Fig. 14b). The phase difference between the $\Delta\phi = 210$ and $\Delta\phi = 90$ deg pressure records is clearly visible. Overall, pressure amplitudes just downstream of the flap-shoulder slot are small (note scale) and combined control does not have a significant effect on the amplitudes (Fig. 14d). Here, the largest amplitude is associated with $\Delta\phi = 90$ deg and the smallest with $\Delta\phi = 210$ deg. The smaller fluctuations may be associated with a larger degree of boundary-layer attachment, and vice versa. More insight into the flow over the flap will be gained from PIV measurements shown in Sec. IV.D.

Comparing plenum pressures in Figs. 14a and 14b indicates phase differences approximately 45 deg different to those of the voltage drive signal. The reason for this was that the unsteady pressures were not measured at the same spanwise location and this indicated a phase variation along the span. This was confirmed by making two simultaneous unsteady pressure measurements in the aft plenum with one measurement location close to the root and the other close to the tip. It is believed that this had a detrimental effect on wing performance but was unavoidable with perturbations being introduced from one side of the wing. One way of rectifying this in the future is to use internal actuators that eliminate phase variations along the span, e.g., [13].

The lift coefficient as a function of angle of attack was considered for control from the leading edge, flap shoulder, and their combination at $\Delta\phi = 210$ deg (Figs. 15a and 15b). Even angles are for α increasing and odd angles are for α decreasing, as before. Note that leading-edge forcing alone acts like a leading-edge device by increasing the stall angle, whereas flap-shoulder forcing alone simulates additional flap deflection with a simultaneous drag reduction. When forcing is introduced simultaneously, at a phase difference that enhances poststall lift, the effect is similar to the combined effect of a leading-edge device and additional flap deflection with maintained drag reduction.

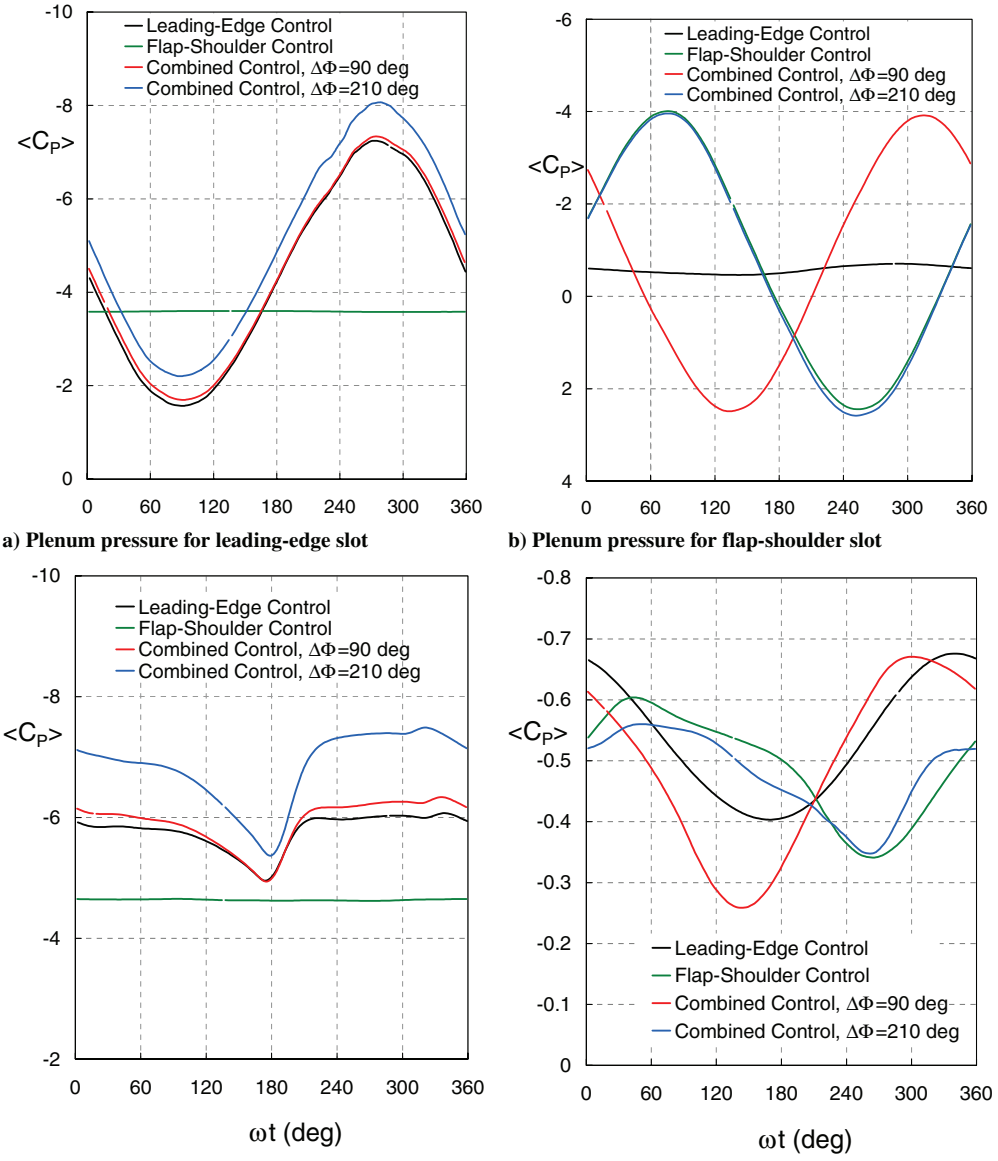

a) Plenum pressure for leading-edge slot

b) Plenum pressure for flap-shoulder slot

c) Surface pressure downstream of leading-edge slot

d) Surface pressure downstream of flap-shoulder slot

Fig. 14 Phase-averaged, unsteady pressures in fore and aft plenums and unsteady surface pressures measured immediately downstream of slots.

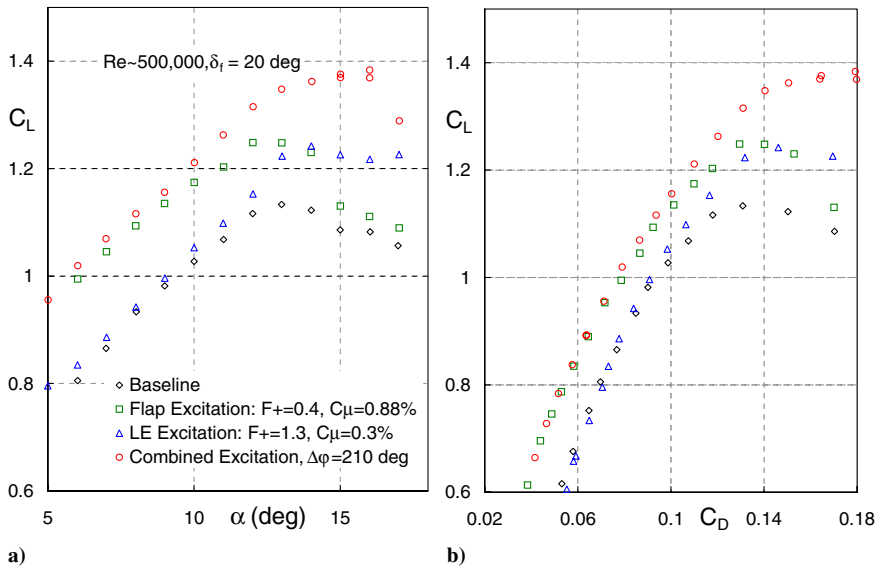

a)

b)

Fig. 15 Overall wing lift illustrating effect of phase when separation is controlled from two locations.

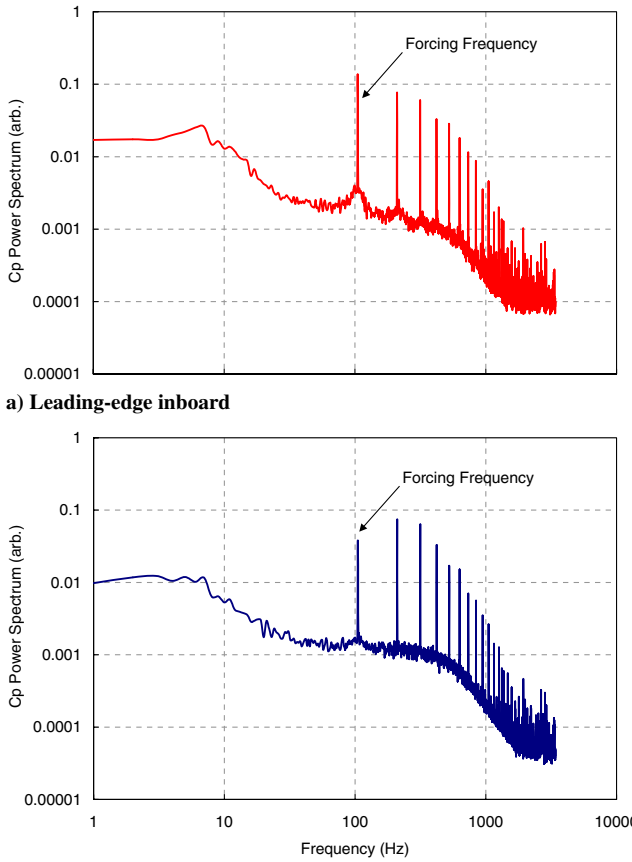

Fig. 16 C_p spectra from unsteady pressure ports located close to leading edge, downstream of slot exit.

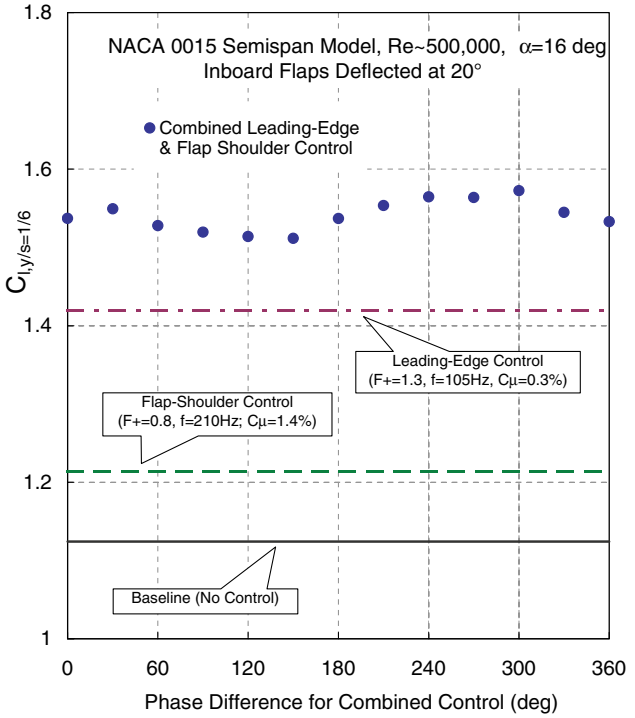

Fig. 17 Poststall inboard lift data showing effect of phase using harmonic control at flap shoulder.

Determining the optimum phase difference empirically, as we have done here, is unavoidable because at present there are no theoretical models that can adequately describe the prevailing flow physics. This applies to both time-mean and unsteady aspects of the problem. When perturbations are used to control separation, a recirculating region (alternatively vortex or bubble) is often present on the surface in a time-mean sense. Even with no periodic perturbations, so-called trapping of a vortex on the surface of a wing has long been recognized and was exploited by Kasper [14,15] to achieve large $C_{L,\max}$ and high aerodynamic efficiency. A number of theoretical models were developed that considered the lift enhancement generated by the vortex as well as its stability above the wing surface [16–18].

The unsteady problem is more complex and it does not appear to have been approached theoretically. Unsteady simulations using a variety of turbulence models, on the other hand, appear to be capable of describing only qualitative time-mean trends providing that the flow under consideration is fully turbulent [19]. The poor predictions are due to the inherent flow complexity, where turbulence coexists with so-called coherent structures, which are usually driven by at least one instability mechanism. Consequently, there are no known models that can adequately calculate the effect of leading parameters such as reduced frequency and perturbation amplitude. For the wing considered in this investigation, the flow is laminar at the leading-edge slot and also may be subjected to competing instability mechanisms due to curvature at the leading-edge region. This would further complicate the present difficulties experienced by computational methods. Recently, however, Rumsey's unsteady Reynolds-averaged Navier–Stokes (URANS) calculations showed that, although the mean flow was poorly predicted, the unsteady pressure oscillations were reasonably well predicted [20]. Thus URANS, and perhaps other models, may serve as a rudimentary design tool for predicting the optimum phase differences.

A further attempt was made to enhance lift by introducing the flap perturbation at the second harmonic of the leading-edge perturbation, i.e., $f_{\text{fs}} = 2f_{\text{le}} = 2 \times 105$ Hz such that $F^+_{\text{le}} = 1.3$ and $F^+_{\text{fs}} = 0.8$. The rationale behind this approach was twofold: first, these frequencies resulted in F^+ values appropriate to both leading-edge and flap-shoulder separation control; second, significant harmonic content was seen to be associated with the perturbations downstream of the leading-edge slot as shown in Figs. 16a and 16b. This approach resulted in a relatively modest dependence of lift on $\Delta\phi$ with two C_l maxima around $\Delta\phi = 30$ and 300 deg at $y/s = 0.167$ (Fig. 17). The largest overall effect, as a function of $\Delta\phi$, was $\Delta C_l = 0.07$ and the maximum C_l was approximately 0.1 less than that attained when $f_{\text{fs}} = f_{\text{le}}$, despite the fact that here the flap shoulder $C_\mu = 1.4\%$. When the flow was controlled with $f_{\text{fs}} \neq nf_{\text{le}}$, n being an integer, significant flow unsteadiness was observed in the vicinity of $C_{L,\max}$.

Additional attempts were made to enhance lift by increasing and decreasing the control frequency in the range of $80 \leq f \leq 155$ Hz, i.e., in the overall F^+ range of 0.33–1.9. Similar results to those shown in the preceding paragraph were obtained for $f = 80$ Hz, but for $f > 105$ Hz the combined effect of control diminished and was indiscernible at $f = 155$ Hz (not shown). This is probably due to the fact that leading-edge generated vortices dissipated in the streamwise direction to the point that they did not interact meaningfully with the vortices generated at the flap shoulder. Control at $F^+_{\text{fs}} < 0.3$, corresponding to $F^+_{\text{le}} < 1.0$, was not attempted because it leads to a phenomenon similar to oscillatory dynamic stall on the flap. Finally, experiments were performed with all flaps deflected at 20 deg (see Sec. IV.E for 40 deg flap deflections). The effect of phase difference inboard was similar to that presented in Figs. 9–15, but virtually no effect was observed near the wing tip (not shown).

A question arises as to whether the sum of the leading-edge and flap-shoulder momentum, if introduced from a single slot (i.e., $C_\mu = 1.18\%$), would deliver comparable aerodynamic performance. In the case of the flap shoulder, prestall ΔC_L varies logarithmically with C_μ (e.g., Fig. 8a) and thus ΔC_L would not be expected to increase any more than an additional $\sim$0.01. This compares unfavorably to the $\Delta C_{L,\max} = 0.13$ which results from adding leading-edge control to flap-shoulder control (Fig. 15a). Because of actuator limitations, $C_\mu \leq 0.88$ for $F^+ = 0.4$, but $C_\mu \leq 1.3\%$ was

achieved at $F^+ = 0.8$ [11] and the logarithmic behavior was similar to that exhibited here. Furthermore, the value of C_μ has no effect on α_s because this is determined by leading-edge separation. At poststall angles, clearly flap-shoulder control will have a minimal impact because the flow is separated at the leading edge. In summary, flap-shoulder control alone cannot deliver similar performance due to the logarithmic variation C_L and its inability to mitigate the leading-edge stall mechanism.

For leading-edge control, increases in amplitude for $C_\mu > 0.5\%$, resulted in significantly nonlinear variation in C_l. Similar observations were made at other reduced frequencies. This behavior was also observed previously on a TAU NACA 0015 airfoil of a similar design [21,22]. The nonlinearity was attributed mainly to the presence of large surface curvature immediately downstream of the slot. This precluded the attainment of performance comparable to that at two locations. Furthermore, it is clearly evident that no amount of leading-edge momentum can attach the flap flow. This conclusion is corroborated by the C_L–C_D polar plot shown in Fig. 15b, where leading-edge control has virtually no effect on the prestall wing drag. In conclusion, single slot momentum equal to the sum of both slots, would not deliver comparable wing performance.

D. Flap Flowfield Measurements

Time-mean contours of spanwise vorticity ($\Omega_y = \partial w/\partial x - \partial u/\partial z$), calculated from two-dimensional PIV measurements above the flap at the wing center span, are shown for the baseline, flap-shoulder, leading-edge, and combined ($\Delta\phi = 210$ deg) control cases in Figs. 18a–18d, respectively ($\alpha = 15$ deg and all flaps are deflected to 20 deg to facilitate optical access for two-dimensional PIV measurements). All control data were computed from the time-mean of phase-averaged results (see Fig. 19); the coordinate system is shown in Fig. 20. The PIV flowfield measurements correlate directly with the center-span lift data shown in Fig. 10b. A much stronger phase dependence was observed further inboard (Fig. 10a), but optical limitations associated with the PIV system precluded the measurement further inboard. For the baseline case, the shear layer separates at the leading edge and consequently is seen to be well above the wing and flap surfaces (Fig. 18a). Flap-shoulder control has very little effect, because the flow is separated upstream at the leading edge (cf. Figs. 18a and 18b). In contrast, leading-edge control deflects the shear layer toward the upper surface of the wing partially attaching it (Figs. 18c) and the flow separates at the flap shoulder. When control is applied at both locations, four effects are evident (Fig. 18d) at the optimum $\Delta\phi$:

1) A region of large vorticity is evident just upstream of the flap shoulder.

2) The shear layer is deflected further toward the flap surface.

3) A region of elevated vorticity is evident near the flap surface at approximately $0.2 < \xi/L_f < 0.4$

4) Positive vorticity near the flap trailing edge diminishes. All of these observations are consistent with the larger lift generated with combined control. Nevertheless, these data as well as the pressure recoveries shown in Fig. 13, illustrate that the shear layer is far from being fully attached to the flap.

Phase-averaged data at $\omega t = 18$, 90, 162, 234, and 306 deg are shown in Fig. 19 for leading-edge control (column 1), as well as combined control for $\Delta\phi = 90$ deg (column 2) and 210 deg (column 3). The drive signal corresponding to control at both locations is shown in Fig. 21; positive and negative values correspond to blowing and suction, respectively. Recall that lift enhancement was minimum and maximum at $\Delta\phi \approx 90$ and 210 deg, respectively (see Figs. 10a and 10b). As noted before, control from the leading edge brings the shear layer closer to the wing surface. These phase-averaged data show the shear layer "flapping" above the surface of the flap; the simplified notion of discrete vortices hypothesized with respect to Fig. 1 does not appear to be accurate. The shear layer is closest to the surface at $\omega t \approx 90$ deg and furthest at $\omega t \approx 306$ deg. Columns 2 and 3 show combined control at different phases (ωt) with respect to the leading-edge blowing cycle. At

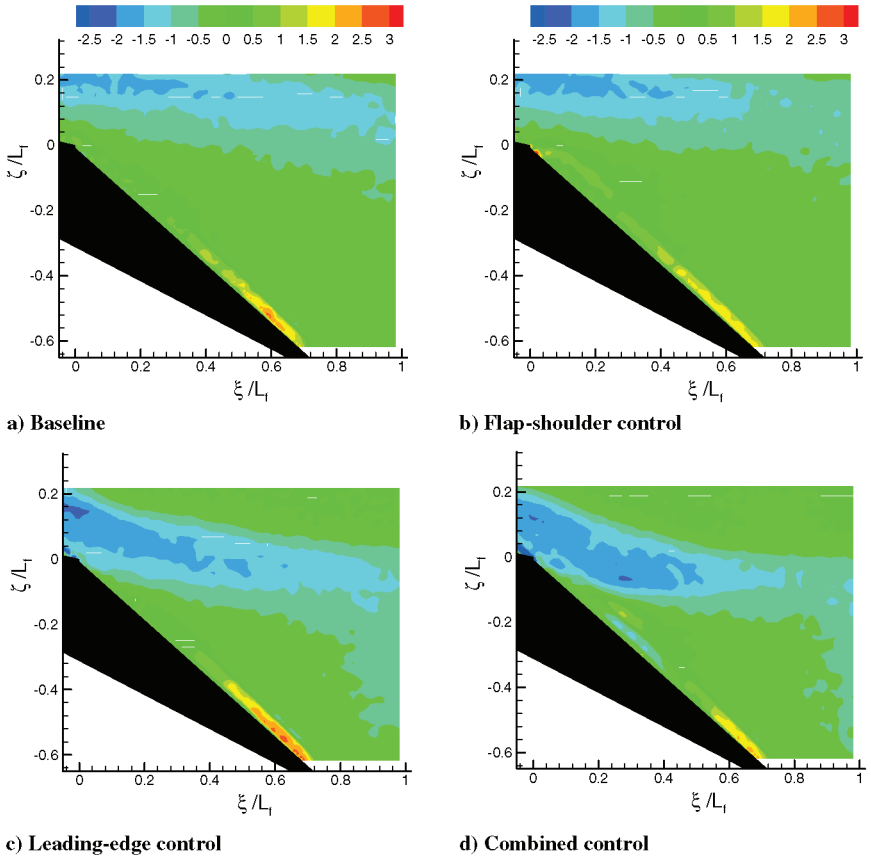

Fig. 18 Time-mean spanwise vorticity contours [$\Omega(\xi, \zeta)$; $s^{-1} \times 10^3$] from two-dimensional time-mean PIV measurements above the flap at $y/s = 0.5$.

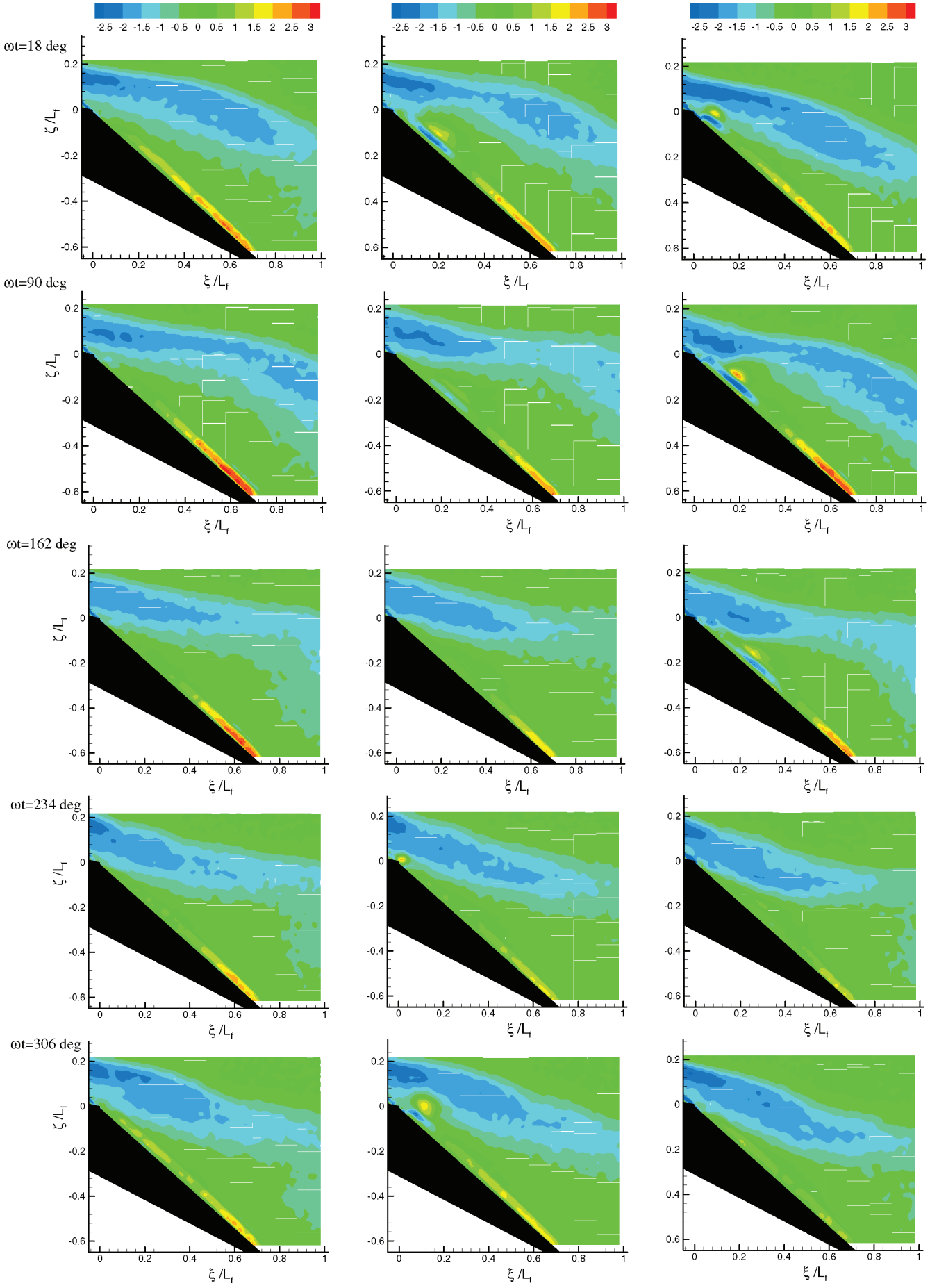

Fig. 19 Phase-averaged spanwise vorticity contours [$\langle\Omega(\xi,\zeta)\rangle; s^{-1} \times 10^3$] from two-dimensional PIV measurements above the flap at $y/s = 0.5$.

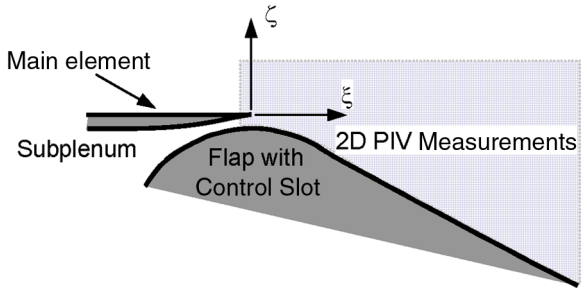

Fig. 20 Close-up section of the center-span flap-slot region, PIV measurement area and coordinate system.

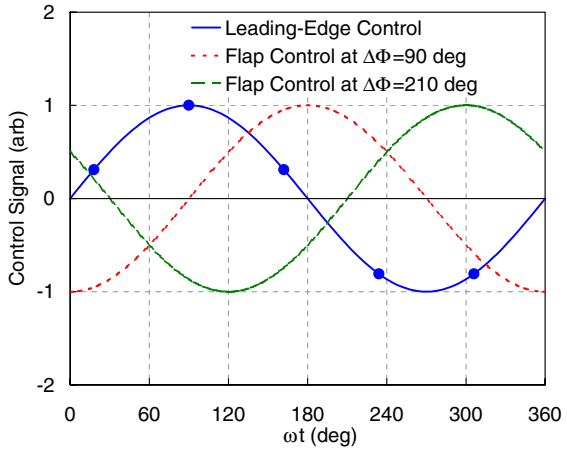

Fig. 21 Leading-edge and flap-shoulder driving signals for combined control. Symbols indicated PIV phases in Fig. 19.

$\Delta\phi = 90$ deg, control from the flap generates two counter-rotating vortices close to the slot (see $\omega t = 306$ and 18 deg). These counter-rotating vortices resemble the discharge of a zero mass-flux jet into quiescent fluid, except here the pair is convected downstream. Control from the flap-shoulder slot alone (not shown here) produced a similar vortex pair close to the slot, but the counterclockwise vortex was significantly stronger than the clockwise vortex (not shown). Nevertheless, this vortex almost completely dissipated by $\xi/L_f = 0.1$. In contrast, for $\Delta\phi = 90$ deg, the vortices have similar strength and the pair is still discernible at $\omega t = 90$ deg. Note that the vortices begin to develop toward the end of the flap-shoulder blowing cycle ($\omega t = 234$ deg) and are shed during the suction cycle. Qualitatively similar observations are made for $\Delta\phi = 210$ deg, but here the clockwise vortex is clearly stronger, with a larger ξ extent, and remains detectable for longer. The generation of a stronger clockwise vortex, which more effectively transports higher momentum flow toward the flap surface, is fully consistent with the load measurements shown in Fig. 10b. This also results in the shear layer, partially deflected by leading-edge control, being deflected closer to the flap surface. A comparison of the two cases near their respective peak suction phases ($\omega t = 306$ and 90 deg for $\Delta\phi = 90$ and 210 deg, respectively) seems to indicate that optimum control occurs when the peak flap-shoulder suction corresponds to the phase at which the shear layer, which emanated from the leading edge, is closest to the wall. The flapping action therefore occurs closer to the wall, bringing the shear layer lower. Even though combined control at $\Delta\phi = 90$ deg is least effective, it is more effective than control from either the leading-edge or flap-shoulder slots individually (see Figs. 10a and 10b). Clearly, measurements further inboard would have produced a more visible difference between the two phase differences.

E. Simplified High-Lift System

A simplified high-lift configuration was investigated by deflecting all wing flaps to 40 deg. It was determined that relatively large control amplitudes $1 < C_\mu \leq 2\%$ were required at the flap for significant lift increments, and with the present setup limitations these could only be achieved at a lower Reynolds number ($Re = 250,000$). This necessitated a commensurate reduction in the control frequency, namely $f = 52.5$ Hz, resulting in the same reduced frequencies as at $Re = 500,000$.

C_p distributions at four spanwise locations on the wing are shown for flap control at low α, starting closest inboard ($y/s = 0.167$, Fig. 22a) and moving progressively outboard to the tip ($y/s = 0.99$, Fig. 22d). As expected, inboard (Figs. 22a and 22b) separation control results in almost complete pressure recovery and circulation increases. As the tip is approached ($y/s = 0.833$, Fig. 22c), the shoulder suction peak and trailing pressures increase, but the overall circulation at this section of the wing diminishes somewhat. At the wing tip (Fig. 22d), the pressure signature is materially different to those inboard. The large $-C_p$ aft at the tip are consistent with a strong vortex that is rolled up, or rolling up, on the flap. Also, the overall wing circulation, i.e., changes to the upper surface main-element pressures, is small to negligible. One can conclude that this is a form of "vortex lift" where the vortex lies approximately parallel to the freestream. In this sense it is similar, in some respects, to vortex lift on a delta wing, although without active control this flowfield does not exist at these large flap deflections.

An unexpected consequence of this is that the lift increment generated at the tip exceeds that generated inboard where the flow is substantially two-dimensional, although the absolute C_l is lower. For example, with flap-shoulder control alone at $\alpha = 0$: $\Delta C_l \approx 0.5$ at $y/s = 0.167$ (Fig. 22a) vs $\Delta C_l \approx 0.7$ at $y/s = 0.99$ (Fig. 22d). Nevertheless, it is doubtful that the tip vortex could be exploited to provide a meaningful fraction of the lift for a simplified high-lift system, because its effect is confined to the region close to the tip and its effectiveness diminishes with increasing α (Fig. 23). Perhaps this type of vortex lift could be exploited on wings of smaller aspect ratio, where the vortex comprises a larger fraction of the span. Nevertheless, such lift generation should not be expected to be efficient (in the sense of L/D), due to the combination of relatively large $-C_p$ on a highly deflected flap with very little change to the circulation as shown by the main-element pressures (Fig. 22d).

With perturbations introduced from both the leading edge and flap shoulder, the poststall phase-dependent lift was similar to that observed previously at smaller flap deflections (all flaps to 20 deg), namely $\Delta C_L \approx 0.2$, despite the larger flap deflection (e.g., Fig. 24). Nevertheless, the overall lift was higher, attaining $C_l \approx 2$ for much of the wingspan. In the vicinity of the wing tip, the sensitivity to phase difference diminished significantly, most probably due to the total breakdown of flow two-dimensionality in this region. The integrated wing lift shown in Fig. 25 indicates that combined control produces $\Delta C_{L,\max} \approx 0.44$ vs 0.24 for all flaps deflected to 20 deg. Consequently, there may be room for further improvement with even larger flap deflection, unfortunately outside of the range possible on the present model. Although further flap deflections may produce more lift, there are certain limitations. First, with simple flaps, the projected planform area *decreases* with flap deflection, whereas on a conventional high-lift system comprising Fowler flaps and leading-edge devices, the projected wing area *increases* with flap and slat deflections. This problem may be exacerbated when leading-edge droop is also included in the high-lift system [7]. Second, the larger flap deflections require ever-larger momentum coefficients to produce meaningful lift enhancements and will put further demands on the already difficult task of providing sufficient actuation authority.

V. Conclusions and Recommendations

This paper considered active separation control from two locations on a semispan wind-tunnel model. Leading-edge perturbations simulated, to some degree, the effect of a leading-edge device and flap-shoulder perturbations simulated additional flap deflection with drag reduction. Surface pressure and flowfield measurements showed that correct phasing between remote active slots is an important factor for maximizing aerodynamic performance. A

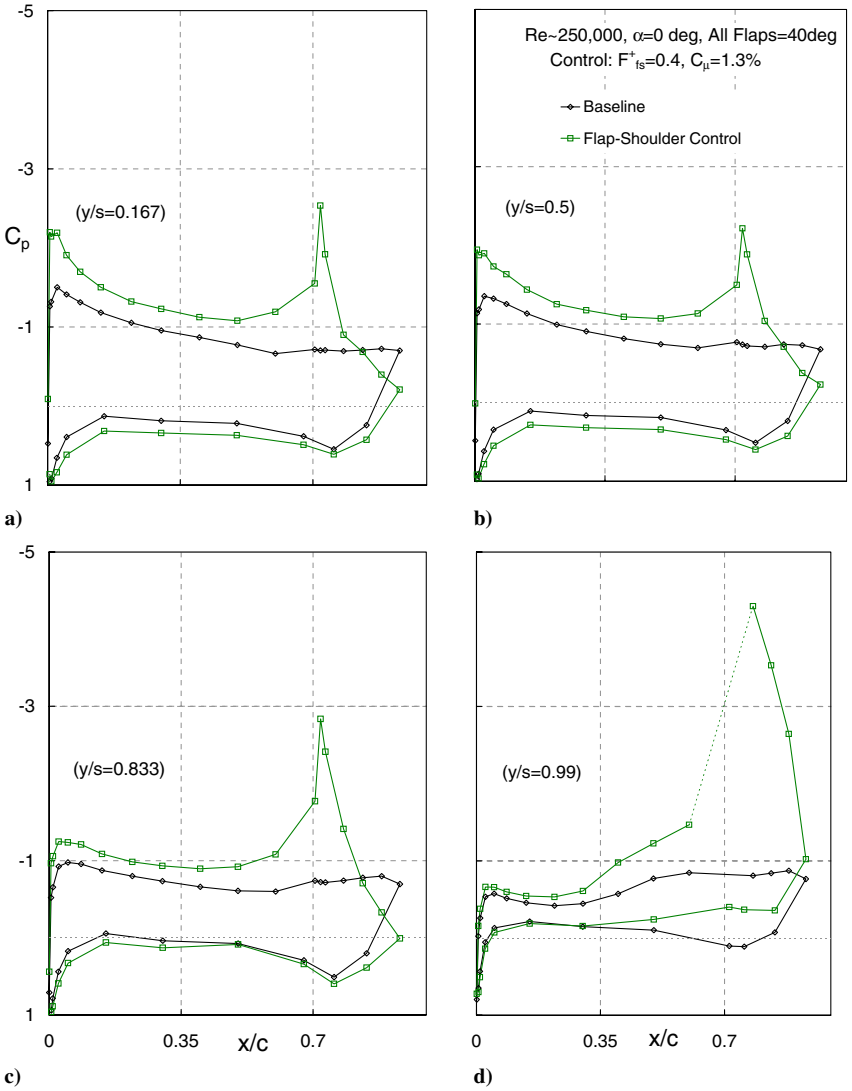

Fig. 22 Comparison of pressure distributions at various spanwise locations with large flap deflection.

guideline was suggested that involves phasing the suction part of flap-shoulder control with the minimum shear layer proximity to the flap surface. The finite flap span did not materially affect the efficacy of control either inboard in the vicinity of the junction vortex, or outboard in the vicinity of the flap-edge vortex. With larger flap deflections, greater $C_{L,\max}$ was achieved, and the lift increment as a result of the phase difference was approximately the same. The sensitivity to perturbation phase difference, however, diminished significantly toward the wing tip.

To further exploit the possible benefits of simplified high-lift, the following suggestions are made:

1) As part of design, the length scales $X_{le} - X_{fs}$ and X_{fs} should be rendered approximately equal. This will allow F^+ based on these length scales to be similar for a given forcing frequency. This can be

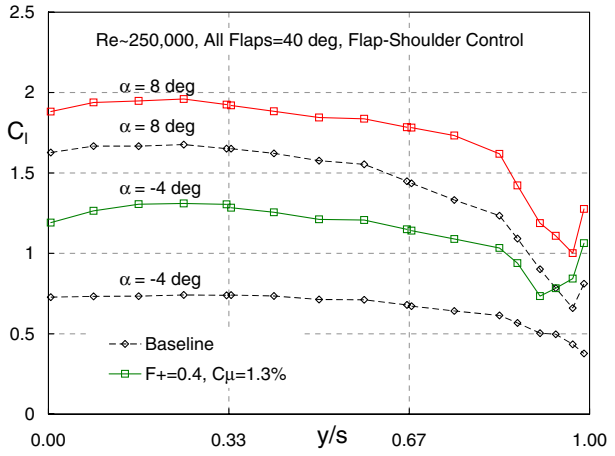

Fig. 23 Spanwise load distribution on the semispan model with large flap deflection at two angles of attack.

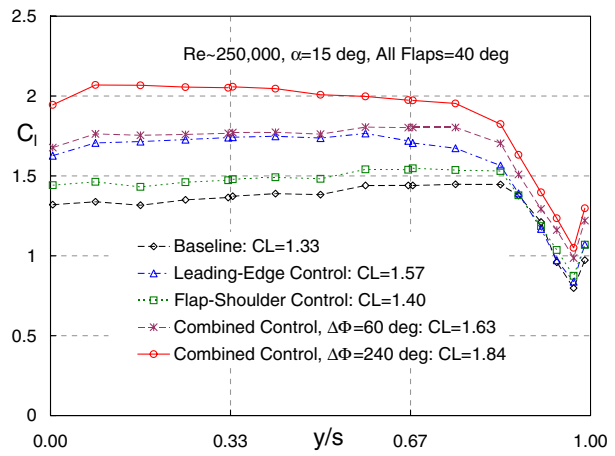

Fig. 24 Poststall wing span-loading with large flap deflections showing the effect of phase when separation is controlled from two locations.

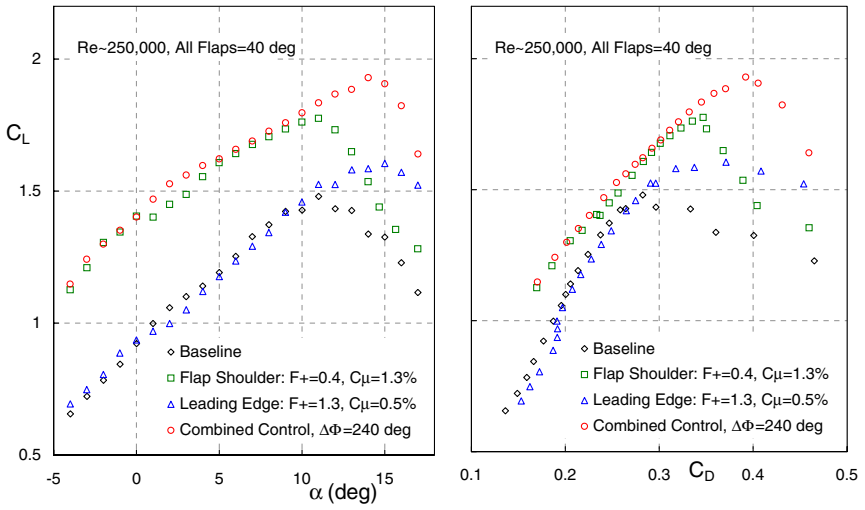

a) b)

Fig. 25 Integrated wing lift illustrating the effect of phase difference on a simplified high-lift system.

achieved, for example, using a longer flap, or by means of a drooped nose in conjunction with a longer flap [7].

2) A study should be made of superimposing mean mass flux (i.e., blowing or suction) on the perturbations. This may have consequences for circulation-control systems that attempt to use pulsed blowing [23]. Combinations of overall zero net mass flux can be investigated, such as, for example, by employing net suction at the flap shoulder with net blowing at the leading edge.

3) Low aspect ratio wings may be able to benefit from the observed tip vortex lift, which is an intensification of the partially rolled-up tip vortex that results from the two-dimensional perturbations.

4) The slot forcing two-dimensionality should be improved by means of internally mounted actuators that eliminate phase variations along the span.

Acknowledgments

This work was performed while the author held a National Research Council–NASA Langley Research Center Associateship. The author wishes to thank W. L. Sellers III, A. E. Washburn, C. S. Yao, L. P. Melton, L. N. Jenkins, I. J. Wygnanski (University of Arizona), and H. M. Nagib (Illinois Institute of Technology, Chicago) for their active assistance and many fruitful discussions. The author also wishes to thank R. D. White, A. Barnes, and J. Harris for their exceptional technical support.

References

[1] Greenblatt, D., and Wygnanski, I., "Control of Separation by Periodic Excitation," *Progress in Aerospace Sciences*, Vol. 36, No. 7, 2000, pp. 487–545.

[2] Seifert, A., and Pack, L. G., "Oscillatory Control of Separation at High Reynolds Numbers," *AIAA Journal*, Vol. 37, No. 9, Sept. 1999, pp. 1062–1071.

[3] Nagib H., Kiedaisch J., Wygnanski, I., Stalker, A., Wood, T., and McVeigh, M., "First-in-Flight Full-Scale Application of Active Flow Control: The XV-15 Tiltrotor Download Reduction," Presented at the *Research and Technology Organization AVT-111 Specialists' Meeting on Enhancement of NATO Military Flight Vehicle Performance by Management of Interacting Boundary Layer Transition and Separation, Prague, Czech Republic*, Paper 29, Oct. 2004.

[4] Weisbrot, I., "Mixing Layer Excited by Two Frequencies," M.S. Thesis, Tel-Aviv Univ., Israel, 1985.

[5] Wygnanski, I., and Petersen, R. A., "Coherent Motion in Excited Free Shear Flows," *AIAA Journal*, Vol. 25, No. 2, 1987, pp. 201–213.

[6] Long, T. A., and Petersen, R. A., "Controlled Interactions in a Forced Axisymmetric Jet. Part 1: Distortion of the Mean Flow," *Journal of Fluid Mechanics*, Vol. 235, 1992, pp. 37–55.

[7] Pack-Melton, L., Yao, C., and Seifert, A., "Application of Excitation from Multiple Locations on a Simplified High-Lift System," *2nd AIAA Flow Control Conference, Portland, OR*, AIAA Paper 2004-2324, 2004.

[8] Naveh, T., Seifert, A., Tumin, A., and Wygnanski, I., "Sweep Effect on Parameters Governing Control of Separation by Periodic Excitation," *Journal of Aircraft*, Vol. 35, No. 3, 1998, pp. 510–512.

[9] Margalit, S., Greenblatt, D., Seifert, A., and Wygnanski, I., "Active Flow Control of a Delta Wing at High Incidence Using Segmented Piezoelectric Actuators," *1st Flow Control Conference, St. Louis, MO*, AIAA Paper 2002-3270, 2002.

[10] Khorrami, M. R., Berkman, M. E., Li, F., and Singer, B. A., "Computational Simulations of a Three-Dimensional High-Lift Wing," *20th AIAA Applied Aerodynamics Conference, St. Louis, MO*, AIAA Paper 2002-2804, 2002.

[11] Greenblatt, D., "Managing Flap Vortices via Separation Control," *AIAA Journal*, Vol. 44, No. 11, 2006, pp. 2755–2764.

[12] Simpson, R. L., "Junction Flows," *Annual Review of Fluid Mechanics*, Vol. 33, Jan. 2001, pp. 415–443.

[13] Greenblatt, D., Paschal, K., Yao, C., and Harris, J., "Separation Control CFD Validation Test Case Part 2: Zero Efflux Oscillatory Blowing," *AIAA Journal*, Vol. 44, No. 12, 2006, pp. 2831–2845.

[14] Kasper, W. A., "Aircraft Wing with Vortex Generation," U.S. Patent No. 3,831,885, August 27, 1974.

[15] Kruppa, W., "Wind Tunnel Investigation of the Kasper Vortex Concept," *Annual Meeting and Technical Display Incorporating the Forum on the Future of Air Transportation, 13th, Washington, D.C.*, AIAA Paper 77-310, 1977.

[16] Rossow, V. J., "Lift Enhancement by an Externally Trapped Vortex," *Journal of Aircraft*, Vol. 15, No. 9, 1978, pp. 618–625.

[17] Saffman, P. G., and Sheffield, J. S., "Flow over a Wing with an Attached Free Vortex," *Studies in Applied Mathematics*, Vol. 57, 1977, pp. 107–117.

[18] Chernyshenko, S. I., "Stabilization of Trapped Vortices by Alternating Blowing Suction," *Physics of Fluids*, Vol. 7, No. 4, April 1995, pp. 802–807.

[19] Rumsey, C. L., Gatski, T. B., Sellers, W. L., III, Vasta, V. N., and Viken, S. A., "Summary of the 2004 Computational Fluid Dynamics Validation Workshop on Synthetic Jets," *AIAA Journal*, Vol. 44, No. 2, 2006, pp. 194–207.

[20] Rumsey, C. L., "Reynolds-Averaged Navier–Stokes Analysis of Zero Efflux Flow Control over a Hump Model," *44th AIAA Aerospace Sciences Meeting and Exhibit, Reno, NV*, AIAA Paper 2006-1114, 2006.

[21] Seifert, A., Darabi, A., and Wygnanski, I., "Delay of Airfoil Stall by Periodic Excitation," *Journal of Aircraft*, Vol. 33, No. 4, 1996, pp. 691–698.

[22] Greenblatt, D., and Wygnanski, I., "Dynamic Stall Control by Periodic Excitation Part 1: NACA 0015 Parametric Study," *Journal of Aircraft*, Vol. 38, No. 3, 2001, pp. 430–438.

[23] Jones, G., and Englar, R., "Advances in Pneumatic Controlled High Lift Systems Through Pulsed Blowing," *21st AIAA Applied Aerodynamics Conference, Orlando, FL*, AIAA Paper 2003-3411, 2003.

A. Plotkin
Associate Editor